Temporal dynamics of the alignment of the turbulent stress and strain rate

Joseph G. Ballouz,[1] Perry L. Johnson,[2] and Nicholas T. Ouellette[1,*]
[1]*Department of Civil and Environmental Engineering, Stanford University, Stanford, California 94305, USA*
[2]*Department of Mechanical and Aerospace Engineering, University of California, Irvine, Irvine, California 92697, USA*

(Received 2 September 2020; accepted 27 October 2020; published 13 November 2020)

The flux of energy between scales in turbulence can be cast as the result of the interaction between a turbulent stress and a rate of strain. Efficient energy transfer requires that these two tensors be oriented properly relative to each other, but previous work has shown that the instantaneous alignment between them is poor. Here, we consider the temporal dynamics of this alignment in a direct numerical simulation of isotropic turbulence. We show that the orientation of the stress lags behind that of the strain rate, both at a single location and along trajectories. However, the timescale of the reorientation of the stress in these cases does not follow the expected dynamical scaling with length scale. To capture the proper dynamical scaling, we reformulate the energy flux between scales using the right Cauchy-Green strain tensor and the second Piola-Kirchhoff stress tensor. Our results highlight the key role played by the deformation of fluid elements in the physics of the energy cascade, and suggest that their irreversible deformation is a Lagrangian manifestation of the cascade's broken time-reversal symmetry.

DOI: 10.1103/PhysRevFluids.5.114606

I. INTRODUCTION

The state of fluid flow that we know as "turbulence" is notoriously hard to define precisely, leading many merely to describe its characteristics instead [1]. Turbulent flows are certainly unsteady, rotational, strongly mixing, and dissipative; but not all flows that have these features should be thought of as turbulent. An additional necessary criterion for turbulence is a net flux of energy between interacting scales, from the scales at which it is injected into the flow to those where it is dissipated. When the (three-dimensional) turbulence is fully developed, this flux organizes into the classical Richardson-Kolmogorov energy cascade [2,3]. One of the consequences of the cascade is that time-reversal symmetry remains broken even as the other symmetries of the Navier-Stokes equations are (statistically) restored [4].

Although this broken time-reversal symmetry may seem trivial (after all, the flow is dissipative), detailed and specific manifestations of irreversibility are surprisingly difficult to pinpoint in statistically stationary turbulence in the inertial range at scales far from the forcing or dissipation. This challenge is particularly true in a Lagrangian framework considering individual fluid elements, where typical scaling signatures of the cascade are difficult to detect [5,6]. A notable recent step forward in this direction was the identification of the so-called "flight-crash" mechanism [7], whereby individual fluid elements in stationary turbulence were found to accelerate slowly and decelerate quickly, thus providing an indication of the arrow of time. But another class of Lagrangian

*nto@stanford.edu

signatures of time irreversibility can be found in the tendency of various geometric quantities to align along fluid-element trajectories. For example, even though the extensional strain rate and vorticity are surprisingly poorly aligned instantaneously [8–11], the vorticity at a given time aligns more strongly with the strain rate experienced previously along Lagrangian trajectories [12]. A similar but even stronger effect was seen when considering not the Eulerian strain but a fully Lagrangian measure of stretching [13]. Since in both of these cases the direction of the vorticity lags behind that of the extensional strain rate, the arrow of time is again revealed. However, the alignment of the vorticity and the strain rate is not fully indicative of the energy cascade [14–16], particularly in an instantaneous sense. Nevertheless, a similar asymmetric time lag in geometric alignment along trajectories was found in two-dimensional turbulence for the scale-dependent turbulent stress and strain rate that together drive the flux of energy between scales [17].

Here, we examine the dynamics of the geometric alignment between the scale-dependent turbulent stress and strain rate, and therefore the efficiency of the energy flux between scales [17–19], in a direct numerical simulation of homogeneous and isotropic three-dimensional turbulence. We find that the stress lags behind the strain, both at fixed locations and along fluid-element trajectories. This result both reveals the broken time-reversal symmetry and indicates the direction of the energy cascade. However, the time it takes for these two Eulerian quantities to reach their peak alignment does not follow the expected scaling with length scale, suggesting that comparing two Eulerian quantities at different times is not reflective of the dynamics of turbulence. Thus, we introduce a fully Lagrangian approach by rewriting the energy flux between scales in terms of the Cauchy-Green strain tensor and the second Piola-Kirchhoff stress tensor. We find that these tensors also improve their alignment as they evolve along trajectories, but now with a temporal scaling that obeys the expected form. Our results shed light on how the Eulerian energy cascade is reflected in the Lagrangian evolution of the flow, and in particular show that the local deformation of fluid elements is a key component in addition to unsteadiness and advection. These findings may point to novel directions for turbulence modeling.

We begin below in Sec. II with a more thorough description of the context of our work, the analysis tools we use, and some details of the numerical simulation used to produce our data. In Sec. III, we describe an analysis of the alignment between the turbulent stress and strain rate in Eulerian terms, introducing different kinds of time lags to partially account for the unsteadiness of the flow. As the evidence we will present suggests that this analysis is not sufficient to capture the full dynamics, in Sec. IV we introduce a fully Lagrangian formulation for the energy flux, and show that it does appear to capture the complete dynamical nature of the cascade. Finally, in Sec. V, we summarize our results and provide some concluding thoughts.

II. BACKGROUND AND METHODOLOGY

A. Stress and strain alignment and cascade efficiency

As is well known, the nonlinearity in the Navier-Stokes equations implies that different scales of motion (as quantified by, say, Fourier modes) are coupled. Thus, even when energy or momentum is introduced into a flow at a single scale, the flow can exhibit a broadband response. At a mathematical level, the mechanism by which scales are coupled is straightforward to deduce. Suppose we define an operator $\mathcal{P}$ that removes some of the scales of motion. Applying this operator to the Navier-Stokes equations results in the appearance of the second-rank tensor

$$\tilde{\tau}_{ij} = \mathcal{P}(u_i u_j) - \mathcal{P}(u_i)\mathcal{P}(u_j), \tag{1}$$

where u_i is a component of the velocity field. Here and throughout, we use tildes to indicate quantities defined for the flow after $\mathcal{P}$ has been applied, so that, for instance, $\tilde{u}_i = \mathcal{P}(u_i)$. Because $\tilde{\tau}_{ij}$ is a symmetric second-rank tensor that appears in the projected momentum equation inside a divergence, it is natural to interpret it as a stress—specifically, as the momentum coupling between the scales of motion retained under $\mathcal{P}$ and those removed.

This turbulent stress also appears in the projected energy equation, most importantly in a term given by

$$\tilde{\Pi} = -\tilde{\tau}_{ij}\tilde{s}_{ij}, \tag{2}$$

were $\tilde{s}_{ij}$ is the rate of strain for the projected velocity field (that is, the symmetric part of the projected velocity gradient). Dimensionally, this term is an energy flux, and expresses the flow of energy between the retained and removed scales. Moreover, as we have described previously [17–19], because it is an inner product between a stress and a strain rate, this term can be interpreted as the mechanical work done on the removed scales by the retained scales. This formulation in turn points to the importance of the relative geometric alignment between these two tensors: if they are orthogonal to each other (in the sense that their inner product vanishes), no work can be done and the scale-to-scale energy flux will vanish regardless of the magnitudes of the two tensors.

Quantifying the alignment of the eigenframes of these two tensors is quite complex in three-dimensional space [18], requiring the specification of at least three degrees of freedom such as Euler or gimbal angles. Previously, however, we introduced a simple scalar measure $\tilde{\Gamma}$ of this alignment that we have dubbed the cascade efficiency [17–19]. $\tilde{\Gamma}$ is straightforwardly defined as the ratio of the actual energy flux $\tilde{\Pi}$ observed in the flow to the maximum energy flux that could occur if $\tilde{\tau}_{ij}$ and $\tilde{s}_{ij}$ were optimally aligned. By definition, $-1 \leqslant \tilde{\Gamma} \leqslant 1$, where the sign conveys information about whether the flux is in the expected direction (i.e., toward smaller scales for three-dimensional turbulence) or not. Thus, $\tilde{\Gamma} = 1$ implies a maximally vigorous cascade of energy to small scales, while $\tilde{\Gamma} = -1$ would imply a maximally vigorous inverse cascade to larger scales. Achieving $\tilde{\Gamma} = 1$ requires perfect alignment between the stress and strain rate [19], which we can interpret as the case when all of the turbulent stress goes to drive energy through the cascade. For any $\tilde{\Gamma} < 1$, turbulent stresses are still active but are not optimally used for scale-to-scale energy flux. For this reason (along with its boundedness), we refer to $\tilde{\Gamma}$ as the cascade efficiency.

As we have shown before, when computed instantaneously and averaged over space, this efficiency is surprisingly low; we have found that $\langle\tilde{\Gamma}\rangle \approx 0.2$–$0.25$ (where the angle brackets denote a spatiotemporal average) in both three-dimensional and two-dimensional turbulence [17–19]. For comparison, if the stress and strain rate were perfectly aligned as is assumed in, for example, standard Boussinesq or Smagorinsky closures, we would have $\langle\tilde{\Gamma}\rangle = 1$. Because $\tilde{\Gamma}$ scales out the tensor magnitude, these low values are indicative of typically poor alignment between the stress and strain rate, an observation we will make use of below.

B. Simulation details

A direct numerical simulation of homogeneous isotropic turbulence provided the flow fields for the analysis we present here. A standard pseudospectral method was used to simulate the incompressible Navier-Stokes equations,

$$\frac{\partial u_i}{\partial t} + u_j\frac{\partial u_i}{\partial x_j} = -\frac{\partial p}{\partial x_i} + \nu\nabla^2 u_i + f_i, \tag{3}$$

in a triply periodic domain, where $p(\mathbf{x}, t)$ is the pressure field that projects the velocity field update at each time step to maintain $\boldsymbol{\nabla}\cdot\mathbf{u} = 0$. Time advancement was done using a second-order Adams-Bashforth scheme, and $2\sqrt{2}/3$ wave number truncation with phase-shift dealiasing was used [20]. The force, $\mathbf{f}$, maintains constant kinetic energy in the lowest two wave number shells. The simulation was initialized with a Gaussian velocity field having a model turbulent energy spectrum and was run for over 10 large eddy turnover times, L/u', until fully developed turbulence was established before computing statistics. The main parameters of the simulation are given in Table I and the energy spectrum of the simulation is shown in Fig. 1.

Lagrangian trajectories were computed from the Eulerian velocity fields by solving the equation of motion for fluid elements (that is, $\dot{\mathbf{x}} = \mathbf{u}$) using a second-order Runge-Kutta scheme. Note that even when we considered the properties of filtered velocity fields (as described below), we always

TABLE I. Characteristics of the isotropic turbulence simulation used for the analysis. The root-mean-square velocity fluctuation is $u' = \sqrt{\langle u_1^2 \rangle}$, the dissipation rate is $\epsilon = 2\nu\langle s_{ij}s_{ij}\rangle$, and the integral length scale is $L = \pi/(2u'^2)\int E(k)/k\,dk$.

N	ν	Δt	$k_{\max}$	u'	ϵ	L	η	T	τ_η	Re_λ	$k_{\max}\eta$
256	1.2×10^{-3}	5×10^{-4}	121	0.70	0.12	1.3	0.010	1.9	0.10	160	1.3

compute trajectories using the full velocity field. Thus, the way that fluid elements sample the velocity fields (which is the result of complicated dynamical processes involving all scales of motion and the way they evolve in time) is always the same regardless of what scales of motion of the velocity field we isolate.

C. Filtering and flux computation

To compute the energy flux defined in Eq. (2) in practice, we must make an explicit choice for the projection operator $\mathcal{P}$. Here, as in our previous work [19], we choose to use a low-pass filter so that we can extract the interaction between nearby scales [21–28]. Operationally, we define, for example, a component of the filtered velocity field $\tilde{u}_i$ as

$$\mathcal{P}(u_i) = \tilde{u}_i(\mathbf{x}) = \int G_r(\mathbf{x} - \mathbf{x}')u_i(\mathbf{x}')d\mathbf{x}', \tag{4}$$

where G_r is a filter kernel that suppresses components of the velocity field with spatial scales smaller than r. Other filtered quantities are computed similarly. Our results are qualitatively insensitive to the exact form of G_r [18,24,29,30], particularly in terms of the trends of how quantities vary with the filter scale r. Different types of filters can, however, lead to some quantitative variations. Here, for computational efficiency, we used a simple top-hat filter computed about each point of interest in the velocity fields. Note that because of differences in the amount of backscatter allowed by this filter as compared with the smoothed filters we have used in our previous work [18,19], our average efficiencies are somewhat larger here than we have reported previously. However, the trends we report below for how the efficiencies vary with scale are not influenced by the filter shape.

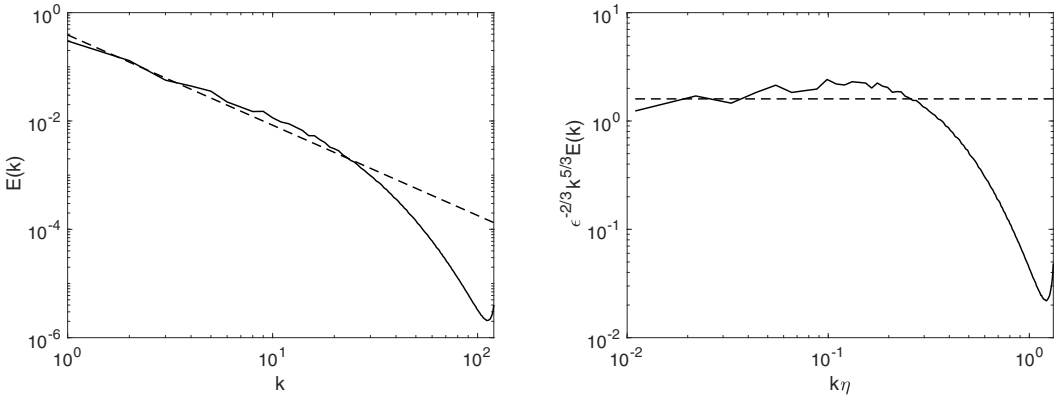

FIG. 1. The energy spectrum $E(k)$, where k is a wave number, plotted both (a) raw and (b) premultiplied, for the direct numerical simulation used for this analysis, with dashed lines showing the inertial range spectrum $E(k) = 1.6\epsilon^{2/3}k^{-5/3}$.

Due to the approximate locality of the turbulent energy cascade and shape of the energy spectrum, this definition of $\mathcal{P}$ allows us to interpret $\tilde{\Pi}$ as the energy flux between scales just larger than r and those just smaller than r [31–33]. Moreover, we note that under this definition, $\tilde{\tau}_{ij}$ is dominated by the largest scales of the unresolved field (that is, the scales just smaller than r), while $\tilde{s}_{ij}$ is dominated by the smallest scales of the resolved field (that is, the scales just larger than r). Finally, note that since in incompressible flow the trace of the turbulent stress $\tilde{\tau}_{ij}$ does not contribute to the energy flux in Eq. (2), we consider here only the deviatoric part of $\tilde{\tau}_{ij}$.

III. TIME-LAGGED EULERIAN QUANTITIES

As remarked above, in general the turbulent stress and strain rate are relatively poorly aligned throughout the inertial range [18,19] and in different types of turbulent flows [34]. These findings are reminiscent of the similar surprising geometric misalignment between the extensional eigenvector of the strain rate and the vorticity vector [8–11]. Instead, the vorticity seems to align preferentially with the intermediate strain-rate eigenvector [8]. Going back to Taylor, it has been suggested that vortex stretching is a good candidate for a physical mechanism that could produce an energy cascade in three-dimensional turbulence [1,35,36]. The idea behind this picture is that when extensional strain stretches a vortex tube along its axis, conservation of angular momentum and of circulation would suggest that the tube should simultaneously thin and increase its rotational speed, thereby energizing smaller scales of motion. If this mechanism were to drive the cascade, one would expect that there ought then to be an observed preferential alignment between the extensional strain-rate eigenvector and the vorticity. Although the intermediate strain-rate eigenvalue is on average positive in turbulence [8], the lack of support in either simulations or experiments for the more efficient vortex stretching that would be produced by alignment with the most extensional eigenvector has thus led to suggestions that vortex stretching is not in fact the principle driver of the energy cascade and that instead processes such as strain self-amplification may play more dominant roles [14–16]. Nevertheless, other studies have found some support for a net alignment of strain rate and vorticity by filtering the velocity field and considering the alignment of the vorticity with the large-scale strain rate only [37] or by considering the different timescales on which these two quantities evolve in turbulence and considering the alignment of the strain rate and vorticity measured at different times [12,13].

Here, we consider a similar notion for the turbulent stress $\tilde{\tau}_{ij}$ and filtered strain rate $\tilde{s}_{ij}$. Instead of computing simply $\tilde{\tau}_{ij}(\mathbf{x}, t)\tilde{s}_{ij}(\mathbf{x}, t)$, where the two tensors are evaluated at the same spatial location $\mathbf{x}$ and time t, we instead first compute the quantity

$$\tilde{\tau}_{ij}(\mathbf{x}, t + \Delta t)\tilde{s}_{ij}(\mathbf{x}, t). \tag{5}$$

That is, we measure the strain rate at a point $\mathbf{x}$ and at a time t and the stress at the same point at a later time $t + \Delta t$. We then use this inner product in place of the instantaneous energy flux to compute a cascade efficiency $\tilde{\Gamma}$, which will now be a function of the time lag Δt. In Fig. 2(a), we show this in-place time-lagged efficiency averaged over $\mathbf{x}$ and t for several different filter scales r. This efficiency is clearly a strong function of Δt for all r. More interestingly, we find that these curves are not symmetric about the origin; rather, they peak at positive values of Δt. Because the efficiency scales out the magnitude of the stress and strain rate and considers only their alignment, this result tells us that, on average, the orientation of the stress eigenframe follows that of the strain rate with a time lag that depends on r. That is, we find that the stress is better aligned with the strain rate in the past than it is with the strain rate at the present time. This asymmetry clearly reveals the broken time-reversal symmetry in the inertial range, but we argue that it also indicates the direction of the energy cascade. As we explained above, the filtered strain rate should be understood as a property of the retained large scales, while the turbulent stress should be understood as a property of the removed small scales. Because we find that the stress lags the strain rate, our results indicate that the small scales follow behind changes in the large scales, just as one would expect. As another point of evidence, we note that our result here is the opposite of what we observed previously in

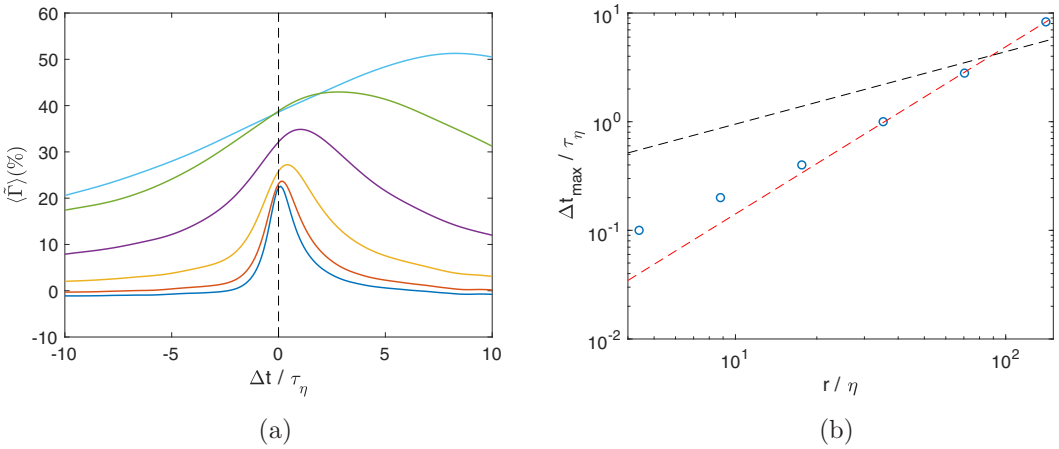

FIG. 2. (a) In-place, time-lagged mean efficiency, computed using the energy flux defined in Eq. (5), as a function of the time lag Δt. Data are shown for filter scales $r = 4.4\eta$, 8.8η, 17.6η, 35.2η, 70.4η, and 140.8η, and the peak efficiency monotonically increases with r. (b) The value of Δt at which the efficiency peaks as a function of filter scale. The black dashed line is a reference $r^{2/3}$ power law; the red line is a best-fit power law with an exponent of 1.5.

two-dimensional turbulence, where the energy cascade reverses direction and drives energy from small to large scales. In that case, we found instead that the strain rate lags behind the stress [17].

The data in Fig. 2(a) show that the peak time-lagged efficiency occurs at a time that grows monotonically with the filter scale r. One might expect that rescaling times by the time at which this peak occurs, which we denote by $\Delta t_{\max}$, and efficiencies by $\tilde{\Gamma}(0)$ might collapse the curves in Fig. 2(a). However, we find (both in this case and for the other cases studied below) that this is not the case, since both the relative magnitude of the peak efficiency and the falloff of the efficiency with time are not independent of scale. Instead, we examine how $\Delta t_{\max}$ itself behaves as a function of r, which we plot in Fig. 2(b). Classical Kolmogorov theory would predict that $\Delta t_{\max}$ should scale like $r^{2/3}$. However, as shown in Fig. 2(b), this is not the scaling we observe. Instead, we find that $\Delta t_{\max} \sim r^{1.5}$. Although the Reynolds number of our simulation is fairly low so that perfect agreement with the expected asymptotic scaling should not be expected, the difference between scaling exponents of $2/3$ and 1.5 is very large—and because the spectrum (Fig. 1) has a reasonably long $-5/3$ scaling range, we would expect the scaling exponent to be close to $2/3$. Additionally, at this Reynolds number and statistical order, this discrepancy is unlikely to be an intermittency effect. Thus, we conclude that even though our results so far correctly display the broken time-reversal symmetry and direction of the cascade, something is missing from our calculations so that our results do not follow the expected dynamical scaling.

A prime candidate for the missing dynamics is advection: in our calculations so far, even though we have computed the stress and strain rate at different times, we have considered only a single spatial point. In reality, however, over the time Δt, the turbulence will sweep past the point $\mathbf{x}$. Thus, it is likely more appropriate to consider

$$\tilde{\tau}_{ij}(\mathbf{X}(t+\Delta t), t+\Delta t)\tilde{s}_{ij}(\mathbf{X}(t), t), \tag{6}$$

where $\mathbf{X}(t)$ is the (Lagrangian) position of a single fluid element at time t. This computation considers the time-lagged stress and strain rate along Lagrangian trajectories, much as was previously done for the vorticity and strain rate [12,13]. Unlike what we computed above, which accounts for the unsteadiness of the flow in only a fairly crude way, tracking the evolution of the stress and strain rate along trajectories captures the local structure of advection.

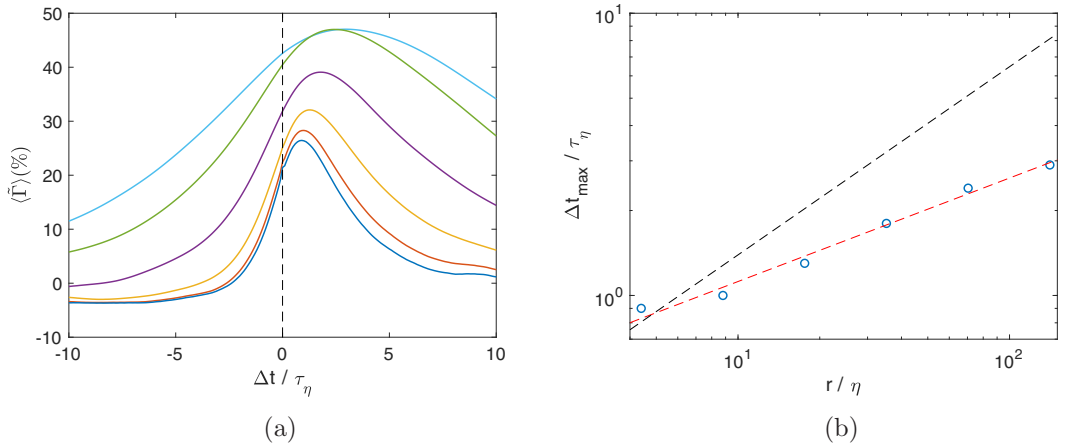

FIG. 3. (a) Time-lagged mean efficiency computed along Lagrangian trajectories using the energy flux defined in Eq. (6), as a function of the time lag Δt. Data are again shown for filter scales $r = 4.4\eta$, 8.8η, 17.6η, 35.2η, 70.4η, and 140.8η, and the peak efficiency monotonically increases with r. (b) The value of Δt at which the efficiency peaks as a function of filter scale. The black dashed line is a reference $r^{2/3}$ power law; the red line is a best-fit power law with an exponent of 0.4.

In Fig. 3(a), we show the mean efficiency (averaged over an ensemble of fluid elements) computed using the inner product defined in Eq. (6) as a function of Δt and for several filter scales. Note that as described above, we always compute the trajectories themselves using the full velocity field (that is, with no filtering) even when considering filtered stresses and strain rates. As with the in-place time-lagged efficiency, we find that these curves are asymmetric about the origin, with the stress again lagging the strain rate, and that the time $\Delta t_{\max}$ at which the peak efficiency occurs increases with scale. But even though it does not qualitatively change our results, accounting for the local nature advection does change them quantitatively. First, we note that the improvement of the efficiency as Δt increases in Fig. 3(a) is in general (aside from the largest filter scale) stronger than what is shown in Fig. 2(a). This makes sense, since both the stress and the strain rate are swept along with the flow as they evolve; thus, the strain rate that the stress is rotating to align with is no longer in the same spatial location after a time Δt has passed. We also find that the scaling of $\Delta t_{\max}$ with r changes when we compute it along trajectories. As shown in Fig. 3(b), for this case we find that $\Delta t_{\max} \sim r^{0.4}$. Although this scaling is closer to the expected dimensional scaling of $r^{2/3}$, it still does not match. As we argue below, this continued discrepancy is a signal that there is a part of the flow dynamics we are still not properly capturing in this formulation.

IV. LAGRANGIAN APPROACH

In addition to being swept along with the flow as time evolves, a fluid element will also experience local straining and rotation such that it may locally deform in addition to being transported. Simply considering statistics along trajectories does not capture this physics. Instead, a fully Lagrangian approach is needed. We note that in many cases, simple advection along trajectories may be sufficient; in this case, however, since we are explicitly interested in stresses and strains that must be referenced to a particular material configuration, we cannot ignore the full dynamics of the flow.

The inner product between the stress and strain rate defined in Eq. (2) is sometimes known as a stress power, and we can use fundamental results in continuum mechanics to rewrite it in a Lagrangian formulation referenced to a given fluid element. To do so, we introduce the deformation gradient tensor F_{ij}, defined as $\partial X_i(t)/\partial x_j$, where again $X_i(t)$ is the Lagrangian position of a fluid

element at time t and $x_i = X_i(0)$ is a reference position at $t = 0$. Physically, it expresses the deformation of a fluid element relative to some initial, reference state. The deformation gradient tensor can then be used to write various types of Lagrangian stresses and strain rates. Here, we will make use of the right Cauchy-Green strain rate and the second Piola-Kirchhoff stress tensor. The right Cauchy-Green strain tensor is defined as

$$E^{(2)}_{ij} = F_{ki}F_{kj}. \tag{7}$$

The corresponding strain rate is given by its time derivative, which can be written in terms of the deformation gradient tensor and the Eulerian strain rate as

$$\dot{E}^{(2)}_{ij} = F_{mi}s_{mn}F_{nj} \tag{8}$$

(where we have omitted a tilde on the Eulerian strain rate s_{ij} as this is a general relation). The second Piola-Kirchhoff stress tensor can similarly be written in terms of the deformation gradient tensor and the Eulerian stress as

$$S^{(2)}_{ij} = JF^{-1}_{im}\tau_{mn}F^{-1}_{jn}, \tag{9}$$

where J is the determinant of the deformation gradient tensor. Note that $J = 1$ for incompressible flow; nevertheless, we include it here for completeness. The Cauchy-Green strain physically encodes the cumulative strain experienced by a fluid element over a time t relative to its reference state at $t = 0$. The eigenvalues of the Cauchy-Green strain express the magnitudes of this strain along its three principle directions. The eigenvectors of the right Cauchy-Green strain tensor point along the directions in the reference state at $t = 0$ that will experience strains given by the corresponding eigenvalues [13]. Note that a left Cauchy-Green strain tensor can also be defined with the same eigenvalues but with eigenvectors that point along the directions that have experienced the corresponding strains in the final state at time t. The Cauchy-Green strains have seen a fair amount of use in recent years in fluid mechanics for the purpose of identifying so-called Lagrangian coherent structures [38]. To our knowledge, the Piola-Kirchhoff stresses have found less application in fluid mechanics. The second Piola-Kirchhoff stress $S^{(2)}_{ij}$, as with any stress, can be seen as a force per unit area. In this case, the relevant force is the ith component of the force acting at time t. The corresponding area, however, is considered in the reference state at time $t = 0$ and at that time has a surface normal that points in the j direction. Thus, importantly for our purposes, both the right Cauchy-Green strain tensor and the second Piola-Kirchhoff stress tensor measure the dynamically evolving forces and deformations of a fluid element but with respect to the reference state of the element before the flow has acted on it.

An additional reason to introduce the right Cauchy-Green strain rate and the second Piola-Kirchhoff stress is that the two form a conjugate pair so that the stress power can be written as

$$\Pi = \tau_{ij}s_{ij} = J^{-1}S^{(2)}_{ij}\dot{E}^{(2)}_{ij}. \tag{10}$$

Thus, using these two tensors we can write the energy flux between scales in a fully Lagrangian way with no approximations. Furthermore, the energy flux written in this way still satisfies the Navier-Stokes equations, while the time-lagged Eulerian fluxes we described above do not. Note that to adapt this expression for our scale-dependent case, we simply use the filtered quantities $\tilde{\tau}_{ij}$ and $\tilde{s}_{ij}$ in the definitions given in Eqs. (8) and (9) and compute $\tilde{\dot{E}}^{(2)}_{ij}$ and $\tilde{S}^{(2)}_{ij}$. We note that there are other conjugate pairs that can be used to write the stress power, such as the first Piola-Kirchoff stress and the deformation gradient tensor. However, using the right Cauchy-Green strain rate and the second Piola-Kirchoff stress is appealing because they share many of the same mathematical properties and thus physical interpretations as the Eulerian stress and strain rates. For example, by construction both the right Cauchy-Green strain rate and the second Piola-Kirchoff stress are symmetric tensors, guaranteeing real eigenvalues and orthogonal eigenvectors.

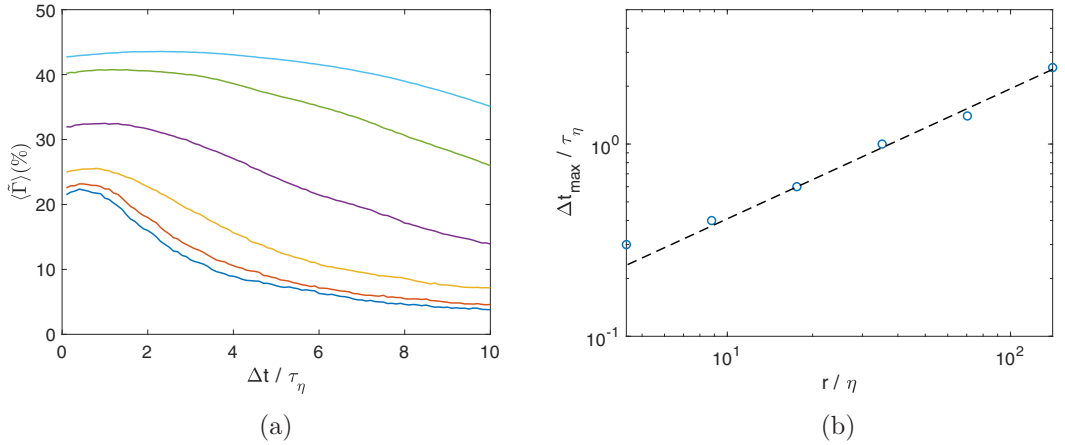

FIG. 4. (a) Mean Lagrangian efficiency computed using the energy flux defined in Eq. (10) as a function of the evolution time Δt. Data are again shown for filter scales $r = 4.4\eta$, 8.8η, 17.6η, 35.2η, 70.4η, and 140.8η, and the peak efficiency monotonically increases with r. (b) The value of Δt at which the efficiency peaks as a function of filter scale. The black dashed line is an $r^{2/3}$ power law.

This Lagrangian formulation of the energy flux between scales allows us to examine, at least indirectly, the contribution of fluid-element deformation to the cascade process. As time evolves, the Cauchy-Green strain and Piola-Kirchhoff stress change both because the flow changes due to unsteadiness and because the fluid element itself deforms. Thus, in contrast to the two efficiencies we defined above where we artificially lagged the Eulerian stress relative to the rate of strain, an efficiency based on $\dot{\tilde{E}}_{ij}^{(2)}$ and $\tilde{S}_{ij}^{(2)}$ arises naturally and exactly from the Navier-Stokes equations and accounts for time evolution, advection along trajectories, and additionally the net deformation of fluid elements induced by the flow.

In Fig. 4(a), we plot this fully Lagrangian efficiency as a function of Δt for several different filter scales, where Δt should now be interpreted as the time the flow has evolved and over which $\dot{\tilde{E}}_{ij}^{(2)}$ and $\tilde{S}_{ij}^{(2)}$ where computed. Because of this slightly different meaning of Δt, we only consider positive values. As with our Eulerian results described above, we find that the alignment, and therefore the efficiency, improves as Δt increases, and then begins to decay again after reaching a peak. In the Lagrangian case, however, when we extract the time at which the peak occurs and plot it against the filter scale, as shown in Fig. 4(b), we find that we recover the expected Kolmogorov scaling of $\Delta t_{\max} \sim r^{2/3}$. Thus, as desired, this fully Lagrangian formulation appears to account for all the relevant flow dynamics.

V. DISCUSSION AND CONCLUSIONS

The recovery of the expected dynamical scaling in this Lagrangian formulation, when combined with the physical meaning of the Cauchy-Green and Piola-Kirchhoff tensors as described above, reveals what was missing from our Eulerian analysis and illuminates a key process in the physics of the energy cascade. As we have argued before, the cascade can be productively conceptualized as a process by which some scales do mechanical work on others [17–19]. In a continuum theory like fluid mechanics, it is natural to think of mechanical work in terms of stresses and strains, but if we were considering a discrete system, we would only need forces and displacements. The difference between the continuum mechanics viewpoint and the particle mechanics picture is the recognition that the shape of an object is fundamentally important for understanding how applied forces will cause it to evolve. Computing stress on a fluid element, for example, requires knowledge both of the applied forces and the orientation of its surface. As time evolves in a fluid flow, the shape of a

fluid element can evolve and deform, and importantly, this is a dynamical process that occurs over finite times. Both of our Eulerian analyses, however, fundamentally neglect this process, instead implicitly assuming that the shape of a fluid element reacts instantaneously to applied stresses since our computations of the Eulerian stress and strain rate are fundamentally instantaneous quantities. Even considering these quantities lagged along trajectories does not address this issue, as such an analysis references the strain rate and stress to different deformational states of the fluid element. In contrast, the Lagrangian formulation properly handles dynamical deformation because both the right Cauchy-Green strain and the second Piola-Kirchhoff stress map the forces and displacements back to the same reference state of the fluid element (namely that at $t = 0$). In a sense, then, the Lagrangian formulation, though seemingly more complex in that it involves quantities less familiar in fluid mechanics, actually allows us to think about simpler quantities such as force and velocity by effectively removing the contributions of deformation by this mapping back to the reference state.

What these results reveal about the dynamical processes occurring along trajectories is that indeed, as one might expect, the effective force that emerges from the coupling between large scales and small scales does tend to align with the velocity of a fluid element on a timescale that follows the expected Kolmogorov scaling. However, during this alignment process, the fluid element also deforms, potentially on a different timescale. The instantaneous stress on the fluid element therefore does not appropriately capture the energy transfer between scales, because even though the instantaneous orientation of the forces on the particle may be relevant for computing the flux, the instantaneous shape of the element may not be. This mismatch between the evolution of force and shape may be part of an explanation for the effective memory that has noted for turbulent stresses and that makes them in a sense viscoelastic [1]. Thus, our results help to clarify the role and importance of deformation in understanding the physics of the cascade.

Additionally, both this deformation and the gradual alignment of the force on a fluid element with its displacement are asymmetric in time and are thus signatures of the broken time-reversal symmetry in turbulence. Indeed, if we measure the cascade efficiency in this Lagrangian formulation in reverse time, we find that it decreases monotonically with no peaks at nonzero Δt. We note that the key role played by deformation in the cascade is similarly implicated in recent work emphasizing the more significant contributions of strain self-amplification relative to vortex stretching in the cascade [14–16].

Taken together, our results allow us to develop an expanded understanding of how the Eulerian energy cascade is manifest in a Lagrangian description of turbulence. In particular, they indicate that there are three essential elements in such a picture. As time progresses, the unsteadiness of the flow drives large-scale straining. This straining in turn drives the production of smaller scale motion via the nonlinearity in the Navier-Stokes equations expressed as a turbulent stress. That this momentum transfer to small scales occurs as a result of the large-scale straining is supported by observation that the orientation of the stress lags behind that of the strain. At the same time, both the stress and strain fields are altered in time due to advection, so that the spatial locations where the energy flux between scales occurs move in time. Advection is organized along the trajectories of fluid elements, and thus the alignment dynamics of the stress and strain rate are more coherent along such trajectories. However, simply considering the Eulerian stress and strain rate along trajectories does not fully capture the dynamics of scale-to-scale energy transfer because this approach does not account for deformation of the fluid elements. And indeed, our results in Sec. IV using a fully Lagrangian formulation of the energy flux between scales indicate that it is necessary to account for this deformation to recover the full dynamics of the cascade. Thus, our results underscore the key role played by deformation in the cascade.

This notion is appealing as it ties back to two key features of the cascade that we raised above: that it retains signatures of the broken time-reversal symmetry even in stationary turbulence and that it can be thought of as a mechanical process of some scales doing work on others. Both of these aspects can be captured by the notion of irreversible deformation: irreversibility naturally breaks time-reversal invariance, and irreversible deformation requires work to be done. Thus, we suggest that the most important element of deformation in the cascade is its irreversible part.

These results suggest some possible avenues that may be fruitful for turbulence modeling. Short-time approximations for the Lagrangian deformation have been used to model the anisotropic part of the pressure Hessian [39] and the turbulent stress [40]. Our results indicate that it may even be valuable to go farther and consider explicit models for the deformation gradient tensor in turbulence closures.

ACKNOWLEDGMENTS

J.G.B. and N.T.O. acknowledge support from the US National Science Foundation under Grant No. CBET-1706950. P.J. acknowledges support from the US Department of Energy's Advanced Simulation and Computing program, Grant No. DE-NA0002373.

[1] H. Tennekes and J. L. Lumley, *A First Course in Turbulence* (MIT Press, Cambridge, MA, 1972).
[2] L. F. Richardson, *Weather Prediction by Numerical Process* (Cambridge University Press, Cambridge, England, 1922).
[3] A. N. Kolmogorov, The local structure of turbulence in incompressible viscous fluid for very large Reynolds numbers, Dokl. Akad. Nauk SSSR **30**, 301 (1941).
[4] G. Falkovich, Symmetries of the turbulent state, J. Phys. A: Math. Theor. **42**, 123001 (2009).
[5] M. Wang, Z. Xiao, C. Meneveau, G. L. Eyink, and S. Chen, Dissipation-energy flux correlations as evidence for the Lagrangian energy cascade in turbulence, Phys. Fluids **22**, 061702 (2010).
[6] G. Falkovich, H. Xu, A. Pumir, E. Bodenschatz, L. Biferale, G. Boffetta, A. S. Lanotte, and F. Toschi, On Lagrangian single-particle statistics, Phys. Fluids **24**, 055102 (2012).
[7] H. Xu, A. Pumir, G. Falkovich, E. Bodenschatz, M. Shats, H. Xia, N. Francois, and G. Boffetta, Flight-crash events in turbulence, Proc. Natl. Acad. Sci. USA **111**, 7558 (2014).
[8] W. T. Ashurst, A. R. Kerstein, R. M. Kerr, and C. H. Gibson, Alignment of vorticity and scalar gradient with strain rate in simulated Navier-Stokes turbulence, Phys. Fluids **30**, 2343 (1987).
[9] A. Tsinober, E. Kit, and T. Dracos, Experimental investigation of the field of velocity gradients in turbulent flows, J. Fluid Mech. **242**, 169 (1992).
[10] A. Vincent and M. Meneguzzi, The dynamics of vorticity tubes in homogeneous turbulence, J. Fluid Mech. **258**, 245 (1994).
[11] V. Borue and S. A. Orszag, Local energy flux and subgrid-scale statistics in three-dimensional turbulence, J. Fluid Mech. **366**, 1 (1998).
[12] H. Xu, A. Pumir, and E. Bodenschatz, The pirouette effect in turbulent flows, Nat. Phys. **7**, 709 (2011).
[13] R. Ni, N. T. Ouellette, and G. A. Voth, Alignment of vorticity and rods with Lagrangian fluid stretching in turbulence, J. Fluid Mech. **743**, R3 (2014).
[14] M. Carbone and A. D. Bragg, Is vortex stretching the main cause of the turbulent energy cascade? J. Fluid Mech. **883**, R2 (2020).
[15] P. L. Johnson, Energy Transfer from Large to Small Scales in Turbulence by Multiscale Nonlinear Strain and Vorticity Interactions, Phys. Rev. Lett. **124**, 104501 (2020).
[16] A. Vela-Martín and J. Jiménez, Entropy, irreversibility and cascades in the inertial range of isotropic turbulence, arXiv:2005.03602.
[17] L. Fang and N. T. Ouellette, Advection and the Efficiency of Spectral Energy Transfer in Two-Dimensional Turbulence, Phys. Rev. Lett. **117**, 104501 (2016).
[18] J. G. Ballouz and N. T. Ouellette, Tensor geometry in the turbulent cascade, J. Fluid Mech. **835**, 1048 (2018).
[19] J. G. Ballouz and N. T. Ouellette, Geometric constraints on energy transfer in the turbulent cascade, Phys. Rev. Fluids **5**, 034603 (2020).
[20] G. S. Patterson Jr. and S. A. Orszag, Spectral calculations of isotropic turbulence: Efficient removal of aliasing interactions, Phys. Fluids **14**, 2538 (1971).
[21] M. Germano, Turbulence: The filtering approach, J. Fluid Mech. **238**, 325 (1992).

[22] S. Liu, C. Meneveau, and J. Katz, On the properties of similarity subgrid-scale models as deduced from measurements in a turbulent jet, J. Fluid Mech. **275**, 83 (1994).
[23] G. L. Eyink, Local energy flux and the refined similarity hypothesis, J. Stat. Phys. **78**, 335 (1995).
[24] M. K. Rivera, W. B. Daniel, S. Y. Chen, and R. E. Ecke, Energy and Enstrophy Transfer in Decaying Two-Dimensional Turbulence, Phys. Rev. Lett. **90**, 104502 (2003).
[25] S. Chen, R. E. Ecke, G. L. Eyink, X. Wang, and Z. Xiao, Physical Mechanism of the Two-Dimensional Enstrophy Cascade, Phys. Rev. Lett. **91**, 214501 (2003).
[26] S. Chen, R. E. Ecke, G. L. Eyink, M. Rivera, M. Wan, and Z. Xiao, Physical Mechanism of the Two-Dimensional Inverse Energy Cascade, Phys. Rev. Lett. **96**, 084502 (2006).
[27] Y. Liao and N. T. Ouellette, Spatial structure of spectral transport in two-dimensional flow, J. Fluid Mech. **725**, 281 (2013).
[28] Y. Liao and N. T. Ouellette, Geometry of scale-to-scale energy and enstrophy transport in two-dimensional flow, Phys. Fluids **26**, 045103 (2014).
[29] D. H. Kelley and N. T. Ouellette, Spatiotemporal persistence of spectral fluxes in two-dimensional weak turbulence, Phys. Fluids **23**, 115101 (2011).
[30] Y. Liao and N. T. Ouellette, Long-range ordering of turbulent stresses in two-dimensional flow, Phys. Rev. E **91**, 063004 (2015).
[31] G. L. Eyink, Locality of turbulent cascades, Physica D **207**, 91 (2005).
[32] G. L. Eyink and H. Aluie, Localness of energy cascade in hydrodynamic turbulence. I. Smooth coarse graining, Phys. Fluids **21**, 115107 (2009).
[33] H. Aluie and G. L. Eyink, Localness of energy cascade in hydrodynamic turbulence. II. Sharp spectral filter, Phys. Fluids **21**, 115108 (2009).
[34] C. W. Higgins, M. B. Palange, and C. Meneveau, Alignment trends of velocity gradients and subgrid-scale fluxes in the turbulent atmospheric boundary layer, Bound.-Layer Meteorol. **109**, 59 (2003).
[35] G. I. Taylor, The transport of vorticity and heat through fluids in turbulent motion, Proc. R. Soc. London A **135**, 685 (1932).
[36] G. I. Taylor, Production and dissipation of vorticity in a turbulent fluid, Proc. R. Soc. London A **164**, 15 (1938).
[37] D. Fiscaletti, G. E. Elsinga, A. Attili, F. Bisetti, and O. R. H. Buxton, Scale dependence of the alignment between strain rate and rotation in turbulent shear flow, Phys. Rev. Fluids **1**, 064405 (2016).
[38] G. Haller, Lagrangian coherent structures, Annu. Rev. Fluid Mech. **47**, 137 (2015).
[39] L. Chevillard and C. Meneveau, Lagrangian Dynamics and Statistical Geometric Structure of Turbulence, Phys. Rev. Lett. **97**, 174501 (2006).
[40] Y. Li, L. Chevillard, G. Eyink, and C. Meneveau, Matrix exponential-based closures for the turbulent subgrid-scale stress tensor, Phys. Rev. E **79**, 016305 (2009).